

# SVTRv2: CTC Beats Encoder-Decoder Models in Scene Text Recognition

Yongkun Du<sup>1</sup>, Zhineng Chen<sup>1\*</sup>, Hongtao Xie<sup>2</sup>, Caiyan Jia<sup>3</sup>, Yu-Gang Jiang<sup>1</sup>

<sup>1</sup>School of Computer Science, Fudan University, China

<sup>2</sup>School of Information Science and Technology, USTC, China

<sup>3</sup>School of Computer Science and Technology, Beijing Jiaotong University, China

ykdu23@m.fudan.edu.cn, {zhinchen, ygj}@fudan.edu.cn, htjie@ustc.edu.cn, cyjia@bjtu.edu.cn

## Abstract

Connectionist temporal classification (CTC)-based scene text recognition (STR) methods, e.g., SVTR, are widely employed in OCR applications, mainly due to their simple architecture, which only contains a visual model and a CTC-aligned linear classifier, and therefore fast inference. However, they generally have worse accuracy than encoder-decoder-based methods (EDTRs), particularly in challenging scenarios. In this paper, we propose SVTRv2, a CTC model that beats leading EDTRs in both accuracy and inference speed. SVTRv2 introduces novel upgrades to handle text irregularity and utilize linguistic context, which endows it with the capability to deal with challenging and diverse text instances. First, a multi-size resizing (MSR) strategy is proposed to adaptively resize the text and maintain its readability. Meanwhile, we introduce a feature rearrangement module (FRM) to ensure that visual features accommodate the alignment requirement of CTC well, thus alleviating the alignment puzzle. Second, we propose a semantic guidance module (SGM). It integrates linguistic context into the visual model, allowing it to leverage language information for improved accuracy. Moreover, SGM can be omitted at the inference stage and would not increase the inference cost. We evaluate SVTRv2 in both standard and recent challenging benchmarks, where SVTRv2 is fairly compared with 24 mainstream STR models across multiple scenarios, including different types of text irregularity, languages, and long text. The results indicate that SVTRv2 surpasses all the EDTRs across the scenarios in terms of accuracy and speed. Code is available at <https://github.com/Topdu/OpenOCR>.

## 1. Introduction

As a task of extracting text from natural images, scene text recognition (STR) has garnered considerable interest over

\*Corresponding Author

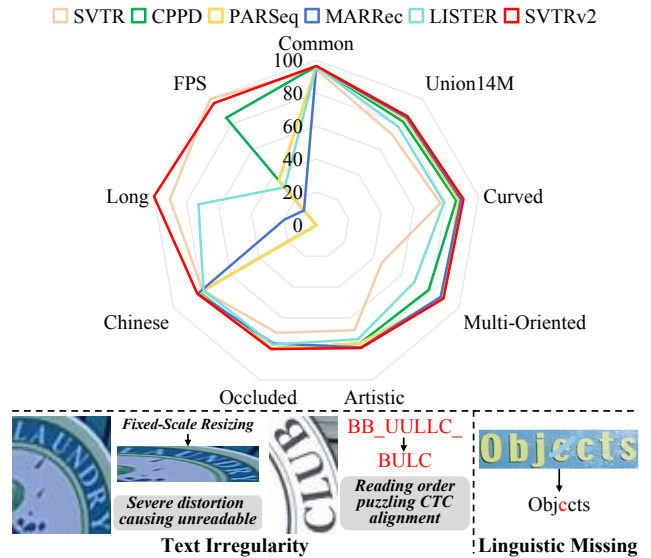


Figure 1. **Top:** comparison with previous methods [4, 8, 11, 12, 25] best in a single scenario, where long text recognition accuracy (Long) and FPS are normalized. Our SVTRv2 achieves the new state of the arts in every scenario except for FPS. Nevertheless, SVTRv2 is still the fastest compared to all the EDTRs. **Bottom:** challenges caused by text irregularity and linguistic missing.

decades. Unlike text from scanned documents, scene text often exists within complex natural scenarios, posing challenges such as background noise, text distortions, irregular layouts, artistic fonts [7], etc. To tackle these challenges, a variety of STR methods have been developed and they can be roughly divided into two categories, i.e., connectionist temporal classification (CTC)-based methods and encoder-decoder-based methods (EDTRs).

Typically, CTC-based methods [11, 23, 28, 39] employ a single visual model to extract image features and then apply a CTC-aligned linear classifier [16] to predict recognition results. This straightforward architecture provides advantages such as fast inference, which makes them especially popular in OCR applications. However, these mod-

els struggle to handle text irregularity, i.e., text distortions, varying layouts, etc. As a consequence, advanced attention-based decoders are introduced as alternatives to the CTC classifier, leading to a series of EDTRs [4, 8, 9, 12, 15, 17, 18, 29, 32, 34, 36, 38, 40, 46–49, 51, 52, 54, 55, 57–59, 62, 63]. These attention-based decoders show appealing performance in integrating multi-modal cues, including visual [12, 48, 52, 58], linguistic [15, 36, 38, 55], and positional [8, 57, 62] ones, which are largely missed in current CTC models. This integration enables EDTRs to perform more effectively in complex scenarios. As depicted in the top of Fig. 1, compared to SVTR [11], a leading CTC model that is adopted by famous commercial OCR engines [28], EDTRs achieve superior results in English and Chinese benchmarks [6, 25], covering challenging scenarios such as curved, multi-oriented, occluded, and artistic text.

Nevertheless, EDTRs are commonly built upon complex architectures, thus sacrificing the inference speed (FPS), as shown in the top of Fig. 1. In addition, besides slower inference speed, EDTRs do not handle long text well. Even LISTER [8], an EDTR dedicated to long text recognition, performs worse than SVTR [11]. Since fast response and recognizing long text are both important for many applications, the OCR community has to face the dilemma that no model excels in accuracy, speed and versatility. When selecting either CTC-based models or EDTRs, users have to accept that the model is inferior in some aspects.

The inferior accuracy of CTC models can be attributed to two primary factors. First, these models struggle with irregular text, as CTC alignment presumes that the text appears in a near canonical left-to-right order [2, 7], which is not always true, particularly in complex scenarios. Second, CTC models seldom encode linguistic information, which is typically accomplished by the decoder of EDTRs. While recent advancements deal with the two issues by employing text rectification [32, 40, 61], developing 2D CTC [44], utilizing masked image modeling [48, 58], etc., the accuracy gap between CTC and EDTRs remains significant, indicating that novel solutions still need to be investigated.

In this paper, we aim to build more powerful CTC models by better handling text irregularity and integrating linguistic context. For the former, we address this challenge by first extracting discriminative features and then better aligning them. First, existing methods uniformly resize text images with various shapes to a fixed size before feeding into the visual model. We question the rationality of this resizing, which easily causes severe distortion of the text, making it unreadable to humans, as shown in the bottom-left of Fig. 1. To this end, we propose a multi-size resizing (MSR) strategy to adaptively resize text images according to their aspect ratios, thus minimizing text distortion and ensuring the discrimination of the extracted visual features. Second, irregular text may be rotated significantly, and the

character arrangement does not align with the reading order of the text, causing the puzzle for CTC alignment, as shown in the bottom-centre example in Fig. 1. To solve this, we introduce a feature rearrangement module (FRM) which rearranges visual features with a horizontal rearrangement, and then identifying and prioritizing relevant vertical features. FRM maps 2D visual features into a sequence aligned with the text’ reading order, thus effectively alleviating the alignment puzzle. Consequently, CTC models integrating MSR and FRM can recognize irregular text effectively, without using rectification modules or attention-based decoders.

As for the latter, the mistakenly recognized example shown in the bottom-right of Fig. 1 clearly highlights the necessity of integrating linguistic information. Since CTC models directly classify visual features, we have to endow the visual model with linguistic context modeling capability, which is less discussed previously. To this end, inspired by guided training of CTC (GTC) [23, 28] and string matching-based recognition [13], we propose a semantic guidance module (SGM), which devises a new scheme that solely leverages surrounding string context to recognize target characters during training. This approach effectively guides the visual model to learn to perceive the linguistic context without rely on decoders. During inference, SGM can be omitted and would not increase the inference cost.

With these contributions, we develop SVTRv2, a novel CTC-based method whose recognition ability has been largely enhanced, while still maintaining a simple architecture and fast inference. To thoroughly validate SVTRv2, we conducted extensive ablation and comparative experiments on benchmarks including standard regular and irregular text [2], occluded scene text [48], the recent Union14M-L benchmarks [25], long text [13], and Chinese [6] text. The results demonstrate that SVTRv2 consistently outperforms all the compared EDTRs across the evaluated scenarios in terms of accuracy and speed, highlighting its effectiveness and broad applicability.

In addition, recent advances [4, 25, 37] revealed the importance of large-scale real-world datasets in improving STR model performance. However, many STR methods primarily derived from synthetic data [19, 24], which fail to fully represent real-world complexities and lead to performance limitations, particularly on challenging scenarios. Notably, we observe that the existing real-world datasets [4, 25, 37] suffer from data leakage, and the results reported in [25] should be updated. As a result, we introduce *U14M-Filter*, a rigorously filtered version of the real-world training dataset Union14M-L [25]. We systematically reproduced and retrained 24 mainstream STR methods from scratch based on *U14M-Filter*. These methods are also thoroughly evaluated across various STR benchmarks. Their accuracy, model size, and inference time constitute a comprehensive and reliable new benchmark for future reference.

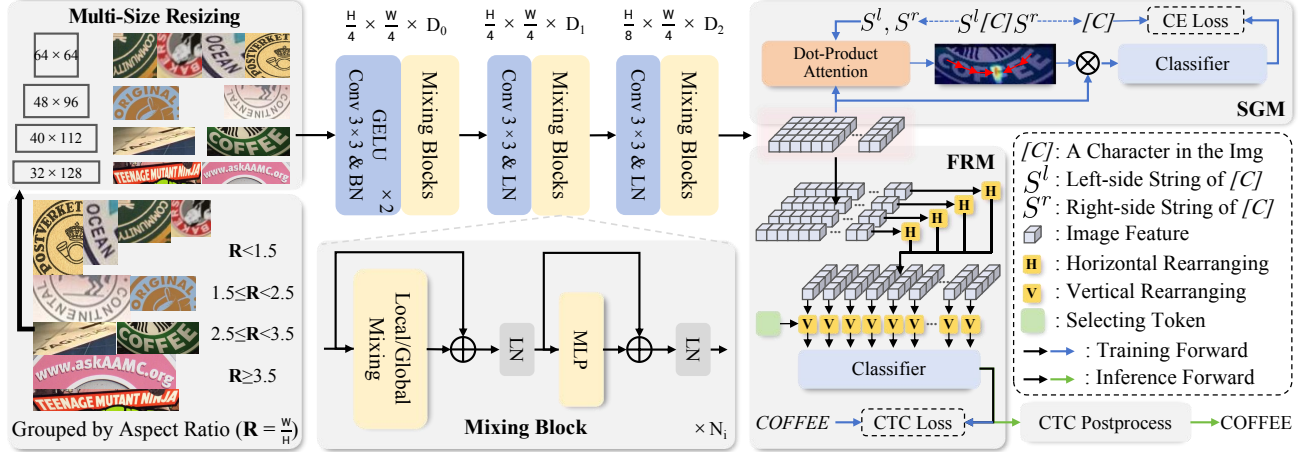


Figure 2. An illustrative overview of SVTRv2. The text is first resized according to multi-size resizing (MSR), then experiences feature extraction. During training both the semantic guidance module (SGM) and feature rearrangement module (FRM) are employed, which are responsible for linguistic context modeling and CTC-oriented feature rearrangement, respectively. Only FRM is retained during inference.

## 2. Related Work

**Irregular text recognition** [1, 25, 35] has posed a significant challenge in STR due to the diverse variation of text instances, where CTC-based methods [11, 23, 28, 39] are often less effective. To address this, some methods [11, 36, 40, 54, 59, 61, 62] incorporate rectification modules [32, 40, 61] that aim to transform irregular text into more regular format. Alternatively, more methods utilize attention-based decoders [29, 38, 47], which employ the attention mechanism to dynamically localize characters regardless of text layout, and thus less affected. However, these methods generally have tailored training hyper-parameters. For instance, the rectification modules [32, 40, 61] typically specify a fixed output image size (e.g.  $32 \times 128$ ), which is not always a suitable choice. While attention-based decoders [29, 38, 47] generally set the maximum recognition length to 25 characters, thus longer text cannot be correctly recognized, as shown in Fig. 5.

**Linguistic Context Modeling.** There are several ways of modeling linguistic context. One major branch is autoregressive (AR)-based STR methods [14, 25, 29, 38, 40, 47, 51, 52, 54, 57, 62, 63], which utilize previously decoded characters to model contextual cues. However, their inference speed is slow due to the character-by-character decoding nature. Some other methods [4, 15, 34, 55] integrate external language models to model the linguistic context and correct the recognition results. While effective, the linguistic context is purely text-based, making it challenging to adapt them to CTC models. There also are some studies [36, 48, 58] to modeling linguistic context with visual information only by using masked image modeling-based pretraining [3, 21]. However, they still depend on attention-based decoders to unleash the linguistic information, not in-

tegrating linguistic cues into the visual model, thus limiting their effectiveness in enhancing CTC models.

## 3. Methods

Fig. 2 illustrates the overview of SVTRv2. A text image is first resized by MSR to the closest aspect ratio, forming the input  $X \in \mathbb{R}^{3 \times H \times W}$ .  $X$  then experiences three consecutive feature extraction stages, yielding visual features  $F \in \mathbb{R}^{\frac{H}{8} \times \frac{W}{4} \times D_2}$ . During training,  $F$  is fed into both SGM and FRM. SGM guides SVTRv2 to model linguistic context, while FRM rearranges  $F$  into the character feature sequence  $\tilde{F} \in \mathbb{R}^{\frac{W}{4} \times D_2}$ , which is synchronized with the text reading order and aligns with the label sequence well. During inference, the SGM is discarded for efficiency.

### 3.1. Multi-Scale Resizing

Previous works typically resize irregular text images to a fixed size, such as  $32 \times 128$ , which, however, may cause undesired text distortion and severely affect the quality of extracted visual features. To address this issue, we propose a simple yet effective multi-size resizing (MSR) strategy that resizes text shapes based on the aspect ratio ( $R = \frac{W}{H}$ ). Specifically, we define four specific sizes:  $[64, 64]$ ,  $[48, 96]$ ,  $[40, 112]$ , and  $[32, \lfloor R \rfloor \times 32]$ , respectively corresponding to aspect ratio:  $R < 1.5$  ( $R_1$ ),  $1.5 \leq R < 2.5$  ( $R_2$ ),  $2.5 \leq R < 3.5$  ( $R_3$ ), and  $R \geq 3.5$  ( $R_4$ ). Therefore, MSR allows text instances adaptively resized under the principles of roughly maintaining their aspect ratios, such that significant text distortion caused by resizing is almost eliminated. As a result, the quality of extracted visual features is guaranteed.

### 3.2. Visual Feature Extraction

Motivated by SVTR [11], the network architecture of SVTRv2 comprises three stages, with stage<sub>*i*</sub> containing  $N_i$  mixing blocks, as illustrated in Fig. 2. To extract discriminative visual features, we devise two types of mixing blocks: local and global. Local mixing is implemented through two consecutive grouped convolutions, which are expected to capture local character features, such as edges, textures, and strokes. Meanwhile, global mixing is realized by the multi-head self-attention (MHSA) mechanism [42]. This mechanism performs global contextual modeling on features, thereby enhancing the model’s comprehension of inter-character relationships and the overall text image. Both the number of groups in the grouped convolution and the number of heads in MHSA are set to  $\frac{D_i}{32}$ . Similar to SVTR, by adjusting hyper-parameters  $N_i$  and  $D_i$ , we can derive three variants of SVTRv2 with different capacities, i.e., Tiny, Small, and Base, which are detailed in Sec. 7 of *Supplementary*.

### 3.3. Feature Rearranging Module

We propose a feature rearrangement module (FRM) to tackle the CTC alignment puzzle arising from rotated text. It rearranges the 2D features  $\mathbf{F} \in \mathbb{R}^{(\frac{H}{8} \times \frac{W}{4}) \times D_2}$  into a feature sequence  $\tilde{\mathbf{F}} \in \mathbb{R}^{\frac{W}{4} \times D_2}$  synchronized with the reading order of the text image. We regard this process as mapping the relevant features from  $\mathbf{F}_{i,j} \in \mathbb{R}^{1 \times D_2}$  to  $\tilde{\mathbf{F}}_m \in \mathbb{R}^{1 \times D_2}$ , where  $i \in \{1, 2, \dots, \frac{H}{8}\}$  and  $j, m \in \{1, 2, \dots, \frac{W}{4}\}$ . This rearrangement can be formalized by a matrix  $\mathbf{M} \in \mathbb{R}^{\frac{W}{4} \times (\frac{H}{8} \times \frac{W}{4})}$ , whereby  $\tilde{\mathbf{F}}$  can be derived from  $\mathbf{M} \times \mathbf{F}$ .

Grounding in the fact that the degree of text curve and rotation can be decomposed into offset components in both horizontal and vertical directions, we propose to learn  $\mathbf{M}$  by using two distinct steps: horizontal rearrangement and vertical rearrangement. As described in Eq. 1, the horizontal one operates on  $\mathbf{F}_i \in \mathbb{R}^{\frac{W}{4} \times D_2}$ , each row in the feature map, to learn a horizontal rearrangement matrix  $\mathbf{M}_i^h \in \mathbb{R}^{\frac{W}{4} \times \frac{W}{4}}$ , where element  $\mathbf{M}_{i,j,m}^h$  represents the probability that the horizontal rearranged feature  $\mathbf{F}_{i,j}^h$  corresponds to the original feature  $\mathbf{F}_{i,m}$ . Based on the learned  $\mathbf{M}_i^h$ , the features in each row are rearranged on the horizontal direction. Subsequently, through a residual and MLP processing, we obtain  $\mathbf{F}^h \in \mathbb{R}^{(\frac{H}{8} \times \frac{W}{4}) \times D_2}$ .

$$\mathbf{M}_i^h = \sigma \left( \mathbf{F}_i \mathbf{W}_i^q (\mathbf{F}_i \mathbf{W}_i^k)^t \right) \quad (1)$$

$$\mathbf{F}_i^{h'} = \text{LN}(\mathbf{M}_i^h \mathbf{F}_i \mathbf{W}_i^v + \mathbf{F}_i), \mathbf{F}_i^h = \text{LN}(\text{MLP}(\mathbf{F}_i^{h'}) + \mathbf{F}_i^{h'})$$

where  $\mathbf{W}_i^q, \mathbf{W}_i^k, \mathbf{W}_i^v \in \mathbb{R}^{D_2 \times D_2}$  are learnable weights,  $\sigma$  is the Softmax function, and  $\mathbf{F}^h = \{\mathbf{F}_1^h, \mathbf{F}_2^h, \dots, \mathbf{F}_{\frac{H}{8}}^h\}$ .

In the following vertical rearrangement, we introduce a selecting token, denoted as  $\mathbf{T}^s \in \mathbb{R}^{1 \times D_2}$ , which simultaneously attends to each column of features  $\mathbf{F}_{:,j}^h \in \mathbb{R}^{\frac{H}{8} \times D_2}$

within  $\mathbf{F}^h$  to learn a vertical rearrangement matrix  $\mathbf{M}_j^v \in \mathbb{R}^{1 \times \frac{H}{8}}$ , as detailed in Eq. 2. The element  $\mathbf{M}_{j,i}^v$  represents the probability that the vertical rearranged feature  $\mathbf{F}_j^v \in \mathbb{R}^{1 \times D_2}$  corresponds to  $\mathbf{F}_{i,j}^h$ . Moreover, all column features share a single selecting token, rather than assigning a unique selecting token to each column feature at different locations. This scheme allows the model to generalize to longer text sequences, even when the number of column features exceeds the number seen during training, thereby facilitating the effective recognition of long text.

$$\mathbf{M}_j^v = \sigma \left( \mathbf{T}^s (\mathbf{F}_{:,j}^h \mathbf{W}_j^k)^t \right), \mathbf{F}_j^v = \mathbf{M}_j^v \mathbf{F}_{:,j}^h \mathbf{W}_j^v \quad (2)$$

where  $\mathbf{W}_j^q, \mathbf{W}_j^k, \mathbf{W}_j^v \in \mathbb{R}^{D_2 \times D_2}$  are learnable weights.

We denote  $\mathbf{F}^v = \{\mathbf{F}_1^v, \mathbf{F}_2^v, \dots, \mathbf{F}_{\frac{W}{4}}^v\} \in \mathbb{R}^{\frac{W}{4} \times D_2}$  as the rearranged feature sequence  $\tilde{\mathbf{F}}$ . Then, the predicted character sequence  $\tilde{\mathbf{Y}}_{ctc} \in \mathbb{R}^{\frac{W}{4} \times N_c}$  is obtained after  $\tilde{\mathbf{F}}$  passes through the classifier  $\tilde{\mathbf{Y}}_{ctc} = \tilde{\mathbf{F}} \mathbf{W}^{ctc}$ , and further aligned with the label sequence  $\mathbf{Y}$  using the CTC rule, where  $\mathbf{W}^{ctc} \in \mathbb{R}^{D_2 \times N_c}$  is the learnable weight of the classifier. Furthermore, to intuitively clarify the role of FRM, we rewrite the mapping relation between  $\tilde{\mathbf{F}}$  and the original feature  $\mathbf{F}$  by the following procedure:

$$\mathbf{F}_{i,j}^h = \mathbf{M}_{i,j}^h \times \mathbf{F}_i = \sum_{w=1}^{\frac{W}{4}} \mathbf{M}_{i,j,w}^h \mathbf{F}_{i,w} \quad (3)$$

$$\begin{aligned} \mathbf{F}_j^v &= \mathbf{M}_j^v \times \mathbf{F}_j^h = \sum_{i=1}^{\frac{H}{8}} \mathbf{M}_{i,j}^v \mathbf{F}_{i,j}^h \\ &= \sum_{i=1}^{\frac{H}{8}} \mathbf{M}_{i,j}^v \sum_{w=1}^{\frac{W}{4}} \mathbf{M}_{i,j,w}^h \mathbf{F}_{i,w} \\ &= \mathbf{M}_j \times \mathbf{F} \end{aligned}$$

$$\mathbf{M}_j = \mathbf{M}_j^v \odot \{\mathbf{M}_{1,j}^h, \mathbf{M}_{2,j}^h, \dots, \mathbf{M}_{\frac{H}{8},j}^h\} \in \mathbb{R}^{1 \times (\frac{H}{8} \times \frac{W}{4})}$$

$$\mathbf{M} = \{\mathbf{M}_1, \mathbf{M}_2, \dots, \mathbf{M}_{\frac{W}{4}}\} \in \mathbb{R}^{\frac{W}{4} \times (\frac{H}{8} \times \frac{W}{4})}$$

$$\tilde{\mathbf{F}} = \mathbf{F}^v = \mathbf{M} \times \mathbf{F} \in \mathbb{R}^{\frac{W}{4} \times D_2} \quad (4)$$

As seen in Eq. 4, the visual features  $\mathbf{F}$ , which fully describe the text to be recognized but may be irregularly organized, are mapped to a more canonical  $\tilde{\mathbf{F}}$ . Different from existing text rectification models [32, 40], which apply geometric transformations at image space and often fail to correct severely irregular text, our FRM is carried out at feature space. It learns a condensed feature sequence  $\tilde{\mathbf{F}}$  by mapping and rearranging the relevant cues from  $\mathbf{F}$  to proper positions in  $\tilde{\mathbf{F}}$ . By employing a structured way that the features are first rearranged horizontally and then vertically, FRM can accommodate text instances with significant irregularities such as large orientation variations, and obtaining features better aligned with the CTC classification.

### 3.4. Semantic Guidance Module

CTC models directly classify visual features to obtain recognition results. This scheme inherently requires that



the linguistic context must be incorporated into visual features, so that the CTC could benefit from. In light of this, we propose a semantic guidance module (SGM) as follows.

For each character  $c_i$  in a text image with character labels  $\mathbf{Y} = \{c_1, c_2, \dots, c_L\}$ , we define its contextual information as the surrounding left string  $\mathbf{S}_i^l = \{c_{i-l_s}, \dots, c_{i-1}\}$  and right string  $\mathbf{S}_i^r = \{c_{i+1}, \dots, c_{i+l_s}\}$ , where  $l_s$  denotes the context window length. The SGM’s role is to guide the visual model to integrate context from both  $\mathbf{S}_i^l$  and  $\mathbf{S}_i^r$  into visual features.

We describe the process using the left string  $\mathbf{S}_i^l$ , with the same process applied symmetrically to the right string  $\mathbf{S}_i^r$ . Firstly, the characters in  $\mathbf{S}_i^l$  are mapped to string embeddings  $\mathbf{E}_i^l \in \mathbb{R}^{l_s \times D_2}$ . Subsequently, these embeddings are encoded to create a hidden representation  $\mathbf{Q}_i^l \in \mathbb{R}^{1 \times D_2}$ , representing the context of the left-side string  $\mathbf{S}_i^l$ . The attention map  $\mathbf{A}_i^l$  is computed by applying a dot product between the hidden representation  $\mathbf{Q}_i^l$  and the visual features  $\mathbf{F}$ , transformed by learned weight matrices  $W^q$  and  $W^k$ . The detailed formulation is as follows:

$$\begin{aligned} \mathbf{Q}_i^l &= \text{LN} \left( \sigma \left( \mathbf{T}^l W^q \left( \mathbf{E}_i^l W^k \right)^t \right) \mathbf{E}_i^l W^v + \mathbf{T}^l \right) \quad (5) \\ \mathbf{A}_i^l &= \sigma \left( \mathbf{Q}_i^l W^q \left( \mathbf{F} W^k \right)^t \right), \quad \mathbf{F}_i^l = \mathbf{A}_i^l \mathbf{F} W^v \end{aligned}$$

where  $\mathbf{T}^l \in \mathbb{R}^{1 \times D_2}$  represents a pre-defined token that encodes the left-side string. The attention map  $\mathbf{A}_i^l$  is used to weight the visual features  $\mathbf{F}$ , producing the feature  $\mathbf{F}_i^l \in \mathbb{R}^{1 \times D_2}$  corresponding to character  $c_i$ . After processing through the classifier  $\tilde{\mathbf{Y}}_i^l = \mathbf{F}_i^l W^{sgm}$ , the predicted class probabilities  $\tilde{\mathbf{Y}}_i^l \in \mathbb{R}^{1 \times N_c}$  for  $c_i$  is obtained to calculate the cross-entropy loss with the label  $c_i$ , where  $W^{sgm} \in \mathbb{R}^{D_2 \times N_c}$  is learnable weights of the classifier.

The weight of the attention map  $\mathbf{A}_i^l$  records the relevance of  $\mathbf{Q}_i^l$  to the visual features  $\mathbf{F}$ , and moreover,  $\mathbf{Q}_i^l$  represents the context of string  $\mathbf{S}_i^l$ . So only when the visual model incorporates the context from  $\mathbf{S}_i^l$  into the visual features of the target character  $c_i$ , the attention map  $\mathbf{A}_i^l$  can maximize the relevance between  $\mathbf{Q}_i^l$  and visual features of the character  $c_i$ , thereby accurately highlighting the corresponding position of character  $c_i$ , as shown in Fig. 3. A similar process applies to the right-side string  $\mathbf{S}_i^r$ , where the corresponding attention map  $\mathbf{A}_i^r$  and visual feature  $\mathbf{F}_i^r$  contribute to the prediction  $\tilde{\mathbf{Y}}_i^r$ . By leveraging the above scheme during training, SGM effectively guides the visual model in integrating the linguistic context into visual features. Consequently, even when SGM is not used during inference, the linguistic context can still be maintained alongside the visual features, and enhancing the accuracy of CTC models. In contrast, previous methods, such as VisionLAN [48] and LPV [58], despite modeling linguistic context using visual features, still rely on attention-based decoders to unleash linguistic information, a process that is incompatible with CTC models.

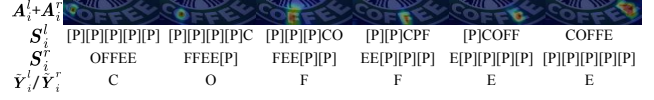


Figure 3. Visualization of attention maps when recognizing the target character by string matching on both sides, where  $l_i$  is set to 5. [P] denotes the padding symbol.

### 3.5. Optimization Objective

During training, The optimization objective is to minimize the loss  $\mathcal{L}$ , which comprises  $\mathcal{L}_{ctc}$  and  $\mathcal{L}_{sgm}$ , as listed below:

$$\begin{aligned} \mathcal{L}_{ctc} &= CTCLoss(\tilde{\mathbf{Y}}_{ctc}, \mathbf{Y}) \quad (6) \\ \mathcal{L}_{sgm} &= \frac{1}{2L} \sum_{i=1}^L (ce(\tilde{\mathbf{Y}}_i^l, \mathbf{c}_i) + ce(\tilde{\mathbf{Y}}_i^r, \mathbf{c}_i)) \\ \mathcal{L} &= \lambda_1 \mathcal{L}_{ctc} + \lambda_2 \mathcal{L}_{sgm} \end{aligned}$$

where  $ce$  represents the cross-entropy loss,  $\lambda_1$  and  $\lambda_2$  are weighting parameters setting to 0.1 and 1, respectively.

## 4. Experiments

### 4.1. Datasets and Implementation Details

We evaluate SVTRv2 across multiple benchmarks covering diverse scenarios. They are: 1) six common regular and irregular benchmarks (*Com*), including ICDAR 2013 (*IC13*) [27], Street View Text (*SVT*) [45], IIIT5K-Words (*IIIT5K*) [33], ICDAR 2015 (*IC15*) [26], Street View Text-Perspective (*SVTP*) [35] and *CUTE80* [1]. For IC13 and IC15, we use the versions with 857 and 1811 images, respectively; 2) the test set of the recent Union14M-L benchmark (*U14M*) [25], which includes seven challenging subsets: *Curve*, *Multi-Oriented (MO)*, *Artistic*, *Contextless (Cless)*, *Salient*, *Multi-Words (MW)* and *General*; 3) occluded scene text dataset (*OST*) [48], which is categorized into two subsets based on the degree of occlusion: weak occlusion (*OST\_w*) and heavy occlusion (*OST\_h*); 4) long text benchmark (*LTB*) [13], which includes 3376 samples of text length from 25 to 35; 5) the test set of BCTR [6], a Chinese text recognition benchmark with four subsets: *Scene*, *Web*, *Document (Doc)* and *Hand-Writing (HW)*.

For English recognition, we train models on real-world datasets, from which the models exhibit stronger recognition capability [4, 25, 37]. There are three large-scale real-world training sets, i.e., the *Real* dataset [4], *REBU-Syn* [37], and the training set of *Union14M-L (U14M-Train)* [25]. However, they all overlap with *U14M* (detailed in Sec. 8 in *Supplementary*) across the seven subsets, leading to data leakage, which makes them unsuitable for training models. To resolve this, we introduce a filtered version of *Union14M-L* training set, termed as *U14M-Filter*, by filtering these overlapping instances. This new dataset is used to train SVTRv2 and 24 mainstream methods we reproduced.

For Chinese recognition, we train models on the training set of *BCTR* [6]. Unlike previous methods that train separately for each subset, we trained the model on an integrated dataset and then evaluated it on the four subsets.

We use AdamW optimizer [30] with a weight decay of 0.05 for training. The LR is set to  $6.5 \times 10^{-4}$  and batchsize is set to 1024. One cycle LR scheduler [43] with 1.5/4.5 epochs linear warm-up is used in all the 20/100 epochs, where a/b means a for English and b for Chinese. For English model, we take SVTRv2 without SGM as the pre-trained and fine-tuned SVTRv2 with SGM with the same above settings. Word accuracy is used as the evaluation metric. Data augmentation like rotation, perspective distortion, motion blur and gaussian noise, are randomly performed and the maximum text length is set to 25 during training. The size of the character set  $N_c$  is set to 94 for English and 6624 [28] for Chinese. In experiments, SVTRv2 means SVTRv2-B unless specified. All models are trained with mixed-precision on 4 RTX 4090 GPUs.

## 4.2. Ablation Study

**Effectiveness of MSR.** We group the *Curve* and *MO* text in *U14M* based on the aspect ratio  $\mathbf{R}_i$ . As shown in Tab. 1, the majority of irregular texts fall within  $\mathbf{R}_1$  and  $\mathbf{R}_2$ , where they are particularly prone to distortion when resized to a fixed size (see *Fixed*<sub>32×128</sub> in Fig. 4). In contrast, MSR demonstrates significant improvements of 15.3% in  $\mathbf{R}_1$  and 5.2% in  $\mathbf{R}_2$  compared to *Fixed*<sub>32×128</sub>. Meanwhile, a large fixed-size *Fixed*<sub>64×256</sub>, although improving the accuracy compared to the baseline, still performs worse than our MSR by clear margins. The results strongly confirm our hypothesis that undesired resizing would hurt the recognition. Our MSR effectively mitigates this issue, providing better visual features thus enhancing the recognition accuracy.

**Effectiveness of FRM.** We ablate the two rearrangement sub-modules (Horizontal (H) rearranging and Vertical (V) rearranging). As shown in Tab. 1, compared to without FRM (w/o FRM), they individually improve accuracy by 2.03% and 0.71% on *MO*, and they together result in a 2.46% gain. Additionally, we explore using a Transformer block (+ TF<sub>1</sub>) to learn the rearrangement matrix holistically, whose effectiveness is less obvious. The most probable reason is that this scheme does not well distinguish between vertical and horizontal orientations. In contrast, FRM performs feature rearrangement in both directions, making it highly sensitive to text irregularity, and thus facilitating accurate CTC alignment. As shown in the left five cases in Fig. 4, FRM successfully recognizes reverse instances, providing strong evidence of FRM’s effectiveness.

**Effectiveness of SGM.** As illustrated in Tab. 2, SGM achieves 0.41% and 2.28% increase on *Com* and *U14M*, respectively, while gains a 5.11% improvement on *OST*. Since *OST* frequently suffers from missing a portion of

		$\mathbf{R}_1$	$\mathbf{R}_2$	$\mathbf{R}_3$	$\mathbf{R}_4$	<i>Curve MO</i>		<i>Com U14M</i>	
		2,688	788	266	32				
SVTRv2 (+MSR+FRM)		87.4	88.3	86.1	87.5	88.17	86.19	96.16	83.86
SVTRv2 (w/o both)		70.5	81.5	82.8	84.4	82.89	65.59	95.28	77.78
vs. MSR (+FRM)	Fixed <sub>32×128</sub>	72.1	83.1	84.1	85.6	83.18	68.71	95.56	78.87
	Padding <sub>32×W</sub>	52.1	71.3	82.3	87.4	71.06	51.57	94.70	71.82
	Fixed <sub>64×256</sub>	76.6	81.6	81.9	80.2	85.70	67.49	95.07	79.03
vs. FRM (+MSR)	w/o FRM	85.7	86.3	86.0	85.5	87.35	83.73	95.44	82.22
	+ H rearranging	87.0	87.1	86.3	85.5	88.05	85.76	95.98	82.94
	+ V rearranging	85.0	87.6	88.5	85.5	88.01	84.44	95.66	82.70
	+ TF <sub>1</sub>	86.4	86.3	87.5	86.1	87.51	85.50	95.60	82.49
-	ResNet+TF <sub>3</sub>	49.3	63.5	64.0	66.7	65.00	42.07	92.26	63.00
	FocalNet-B	56.7	73.2	75.3	73.9	76.46	45.80	94.49	71.63
	ConvNeXtV2	58.4	71.0	73.6	71.2	75.97	45.95	93.93	70.43
	ViT-S	68.5	73.8	73.8	73.0	75.02	64.35	93.57	72.09
	SVTR-B	53.3	74.8	76.4	78.4	76.22	44.49	94.58	71.17
+FRM	ResNet+TF <sub>3</sub>	53.8	67.9	65.5	65.8	69.00	46.02	93.12	66.81
	FocalNet-B	57.1	75.2	77.1	78.4	75.52	51.21	94.39	72.73
	ConvNeXtV2	60.7	79.0	79.0	81.1	79.72	53.32	94.19	73.09
	ViT-S	75.1	79.4	79.0	78.4	80.42	72.17	94.44	77.07
	SVTR-B	59.1	79.0	78.8	80.2	79.84	51.28	94.75	73.48
+MSR	ResNet+TF <sub>3</sub>	68.2	71.3	75.3	72.1	75.64	60.33	93.50	71.95
	FocalNet-B	80.5	80.6	79.2	85.0	82.26	74.82	94.92	78.94
	ConvNeXtV2	76.2	79.0	82.3	80.2	81.05	73.27	94.60	77.71
- / + SGM		<i>OST<sub>w</sub></i>	<i>OST<sub>h</sub></i>	Avg	<i>OST<sub>w</sub>*</i>	<i>OST<sub>h</sub>*</i>	Avg	<i>Com*</i>	<i>U14M*</i>
ResNet+TF <sub>3</sub>		71.6	51.8	61.72	77.9	55.0	66.43	95.19	78.61
FocalNet-B		78.9	62.8	70.88	84.6	70.6	77.61	96.28	84.10
ConvNeXtV2		76.0	58.2	67.10	82.0	63.9	72.97	96.09	82.10

Table 1. Ablations on MSR and FRM (top) and assessing MSR, FRM, and SGM across visual models (lower). \* means with SGM.

		Method	<i>OST<sub>w</sub></i>	<i>OST<sub>h</sub></i>	Avg	<i>Com</i>	<i>U14M</i>
Linguistic context modeling	w/o SGM		82.86	66.97	74.92	96.16	83.86
	SGM		<b>86.26</b>	<b>73.80</b>	<b>80.03</b>	<b>96.57</b>	<b>86.14</b>
	GTC [23]		83.07	68.32	75.70	96.01	84.33
	ABINet [15]		83.07	67.54	75.31	96.25	84.17
	VisionLAN [48]		83.25	68.97	76.11	96.39	84.01
	PARSeq [4]		83.85	69.24	76.55	96.21	84.72
	MAERec [25]		83.21	69.69	76.45	96.47	84.69

Table 2. Comparison of the proposed SGM with other language models in linguistic context modeling on *OST*.

characters, this notable gain implies that the linguistic context has been successfully established. For comparison, we also employ GTC [23] and four popular language decoders [4, 15, 25, 48] to substitute for our SGM. However, there is no much difference between the gains obtained from *OST* and the other two datasets (*Com* and *U14M*). This suggests that SGM offers a distinct advantage in integrating linguistic context into visual features, and significantly improving the recognition accuracy of CTC models. The five cases on the right side of Fig. 4 showcase that SGM facilitates SVTRv2 to accurately decipher occluded characters, achieving comparable results with PARSeq [4], which

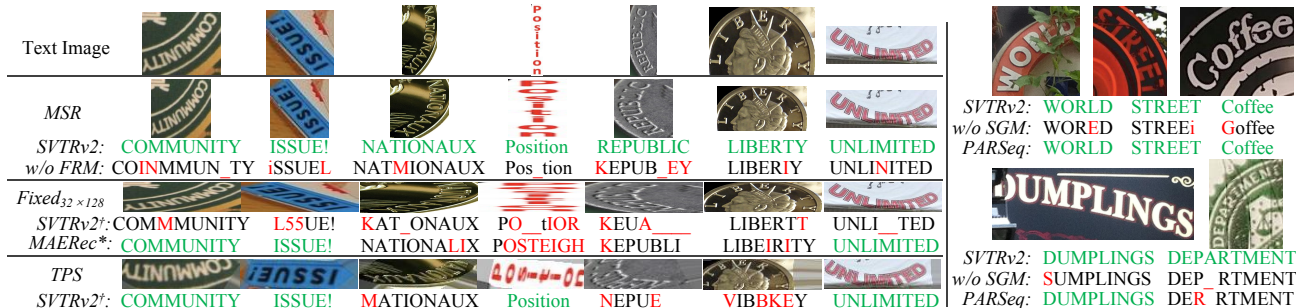


Figure 4. Qualitative comparison of SVTRv2 with previous methods on irregular and occluded text. <sup>†</sup> means that SVTRv2 utilizes the fixed-scale ( $Fixed_{32 \times 128}$ ) or rectification module ( $TPS$ ) as the resize strategy.  $MAERec^*$  means that SVTRv2<sup>†</sup> integrates with the attention-based decoder from the previous best model, i.e. MAERec [25], such a decoder is widely employed in [5, 31, 38, 51, 52, 54, 56]. Green, red, and  $\_$  denotes correctly, wrongly and missed recognition, respectively.

			IIIT5k	SVT	ICDAR2013	ICDAR2015	SVTP	CUTE80		Curve	Multi-Oriented	Artistic	Contextless	Salient	Multi-Words	General						
Method	Venue	Encoder	Common Benchmarks						Avg	Union14M Benchmarks						Avg	$LTB$	$OST$	Size	FPS		
ASTER [40]	TPAMI19	ResNet+LSTM	96.1	93.0	94.9	86.1	87.9	92.0	91.70	70.9	82.2	56.7	62.9	73.9	58.5	76.3	68.75	0.1	61.9	19.0	67.1	
NRR [38]	ICDAR19	Stem+TF <sub>6</sub>	98.1	96.8	97.8	88.9	93.3	94.4	94.89	67.9	42.4	66.5	73.6	66.4	77.2	78.3	67.46	0.0	74.8	44.3	17.3	
MORAN [32]	PR19	ResNet+LSTM	96.7	91.7	94.6	84.6	85.7	90.3	90.61	51.2	15.5	51.3	61.2	43.2	64.1	69.3	50.82	0.1	57.9	17.4	59.5	
SAR [29]	AAAI19	ResNet+LSTM	98.1	93.8	96.7	86.0	87.9	95.5	93.01	70.5	51.8	63.7	73.9	64.0	79.1	75.5	68.36	0.0	60.6	57.5	15.8	
DAN [47]	AAAI20	ResNet+FPN	97.5	94.7	96.5	87.1	89.1	94.4	93.24	74.9	63.3	63.4	70.6	70.2	71.1	76.8	70.05	0.0	61.8	27.7	99.0	
SRN [55]	CVPR20	ResNet+FPN	97.2	96.3	97.5	87.9	90.9	96.9	94.45	78.1	63.2	66.3	65.3	71.4	58.3	76.5	68.43	0.0	64.6	51.7	67.1	
SEED [36]	CVPR20	ResNet+LSTM	96.5	93.2	94.2	87.5	88.7	93.4	92.24	69.1	80.9	56.9	63.9	73.4	61.3	76.5	68.87	0.1	62.6	24.0	65.4	
AutoSTR [59]	ECCV20	NAS+LSTM	96.8	92.4	95.7	86.6	88.2	93.4	92.19	72.1	81.7	56.7	64.8	75.4	64.0	75.9	70.09	0.1	61.5	6.0	82.6	
RoScanner [57]	ECCV20	ResNet	98.5	95.8	97.7	88.2	90.1	97.6	94.65	79.4	68.1	70.5	79.6	71.6	82.5	80.8	76.08	0.0	68.6	48.0	64.1	
ABINet [15]	CVPR21	ResNet+TF <sub>3</sub>	98.5	98.1	97.7	90.1	94.1	96.5	95.83	80.4	69.0	71.7	74.7	77.6	76.8	79.8	75.72	0.0	75.0	36.9	73.0	
VisionLAN [48]	ICCV21	ResNet+TF <sub>3</sub>	98.2	95.8	97.1	88.6	91.2	96.2	94.50	79.6	71.4	67.9	73.7	76.1	73.9	79.1	74.53	0.0	66.4	32.9	93.5	
PARSeq [4]	ECCV22	ViT-S	98.9	98.1	98.4	90.1	94.3	98.6	96.40	87.6	88.8	76.5	83.4	84.4	84.3	84.9	84.26	0.0	79.9	23.8	52.6	
MATR [34]	ECCV22	ResNet+TF <sub>3</sub>	98.8	<b>98.3</b>	97.9	90.3	95.2	97.2	96.29	82.2	73.0	73.4	76.9	79.4	77.4	81.0	77.62	0.0	77.8	44.3	46.9	
MGP-STR [46]	ECCV22	ViT-B	97.9	97.8	97.1	89.6	95.2	96.9	95.75	85.2	83.7	72.6	75.1	79.8	71.1	83.1	78.65	0.0	78.7	148	120	
CPPD [12]	Preprint	SVTR-B	99.0	97.8	98.2	90.4	94.0	<b>99.0</b>	96.40	86.2	78.7	76.5	82.9	83.5	81.9	83.5	81.91	0.0	79.6	27.0	125	
LPV [58]	IJCAI23	SVTR-B	98.6	97.8	98.1	89.8	93.6	97.6	95.93	86.2	78.7	75.8	80.2	82.9	81.6	82.9	81.20	0.0	77.7	30.5	82.6	
MAERec [25]	ICCV23	ViT-S	<b>99.2</b>	97.8	98.2	90.4	94.3	98.3	96.36	89.1	87.1	79.0	84.2	<b>86.3</b>	85.9	84.6	85.17	9.8	76.4	35.7	17.1	
LISTER [8]	ICCV23	FocalNet-B	98.8	97.5	98.6	90.0	94.4	96.9	96.03	78.7	68.8	73.7	81.6	74.8	82.4	83.5	77.64	36.3	77.1	51.1	44.6	
CDistNet [62]	IJCV24	ResNet+TF <sub>3</sub>	98.7	97.1	97.8	89.6	93.5	96.9	95.59	81.7	77.1	72.6	78.2	79.9	79.7	81.1	78.62	0.0	71.8	43.3	15.9	
CAM [54]	PR24	ConvNeXtV2	98.2	96.1	96.6	89.0	93.5	96.2	94.94	85.4	<b>89.0</b>	72.0	75.4	84.0	74.8	83.1	80.52	0.7	74.2	58.7	28.6	
BUSNet [49]	AAAI24	ViT-S	98.3	98.1	97.8	90.2	<b>95.3</b>	96.5	96.06	83.0	82.3	70.8	77.9	78.8	71.2	82.6	78.10	0.0	78.7	32.1	83.3	
OTE [52]	CVPR24	SVTR-B	98.6	96.6	98.0	90.1	94.0	97.2	95.74	<b>86.0</b>	<b>75.8</b>	74.6	74.7	81.0	65.3	82.3	77.09	0.0	77.8	20.3	55.2	
C T C	CRNN [39]	TPAMI16	ResNet+LSTM	95.8	91.8	94.6	84.9	83.1	91.0	90.21	48.1	13.0	51.2	62.3	41.4	60.4	68.2	49.24	47.2	58.0	16.2	172
	SVTR [11]	IJCAI22	SVTR-B	98.0	97.1	97.3	88.6	90.7	95.8	94.58	76.2	44.5	67.8	78.7	75.2	77.9	77.8	71.17	45.1	69.6	18.1	161
			SVTRv2-T	98.6	96.6	98.0	88.4	90.5	96.5	94.78	83.6	76.0	71.2	82.4	77.2	82.3	80.7	79.05	47.8	71.4	5.1	201
			SVTRv2-S	99.0	<b>98.3</b>	98.5	89.5	92.9	98.6	96.13	88.3	84.6	76.5	84.3	83.3	85.4	83.5	83.70	47.6	78.0	11.3	189
		SVTRv2-B	<b>99.2</b>	98.0	<b>98.7</b>	<b>91.1</b>	93.5	<b>99.0</b>	<b>96.57</b>	<b>90.6</b>	<b>89.0</b>	<b>79.3</b>	<b>86.1</b>	86.2	<b>86.7</b>	<b>85.1</b>	<b>86.14</b>	<b>50.2</b>	<b>80.0</b>	19.8	143	

Table 3. All the models and SVTRv2 are trained on  $U14M-Filter$ .  $TF_n$  denotes the  $n$ -layer Transformer block [42].  $Size$  denotes the model size ( $M$ ).  $FPS$  is uniformly measured on one NVIDIA 1080Ti GPU. In addition, we discuss the results of SVTRv2 trained on synthetic datasets [19, 24] in *Supplementary*.

is equipped with an advanced permuted language model.

**Adaptability to different visual models.** We further examine MSR, FRM, and SGM on five frequently used visual models [10, 11, 20, 50, 53]. As presented in the bottom part of Tab. 1, these modules consistently enhance the performance (ViT [10] and SVTR [11] employ absolute positional coding and do not compatible with MSR). When both FRM and MSR modules incorporated, ResNet+TF<sub>3</sub> [20], Focal-

Net [53], and ConvNeXtV2 [54] exhibit significant accuracy improvements, either matching or even exceeding the accuracy of their EDTR counterparts (see Tab. 3). The results highlight the versatility of the three proposed modules.

### 4.3. Comparison with State-of-the-arts

To demonstrate the effectiveness of SVTRv2 in English, we compare it with 24 popular STR methods. All the mod-



els are tested on the newly constructed *U14M* and the results are given in Tab. 3. SVTRv2-B ranks the top in 12 of the 15 evaluated scenarios, It almost outperforms all the EDTRs in every scenario, showing a clear accuracy advantage. Meanwhile, it still enjoys a small model size and a significant speed advantage. Specifically, compared to MAERec, the best-performed existing model on *U14M*, SVTRv2-B shows an accuracy improvement of 0.97% and 8× faster inference speed. Compared to CPPD, which is known for its accuracy-speed tradeoff, SVTR-B runs faster than 10%, along with a 4.23% accuracy increase on *U14M*. Regarding OST, as illustrated in the right part of Fig. 4, SVTR-B relies solely on a single visual model but achieves comparable accuracy to PARSeq, which employed the advanced permuted language model and is the best-performed existing model on OST. In the case of long text recognition, where a large portion of EDTRs are incapable of recognizing, SVTR-B outperforms LISTER, the best EDTR method on LTB, by 13%, demonstrating the remarkable scalability of SVTRv2. In addition, SVTRv2-T and SVTRv2-S, the two smaller models also show leading accuracy compared with models of similar sizes, offering solutions with different accuracy-speed tradeoff.

Two observations are derived when looking into the results on *Curve* and *MO*. First, SVTRv2 models significantly surpass existing CTC models. For example, compared to SVTR-B, SVTRv2-B gains prominent accuracy improvements of 14.4% and 44.5%, respectively. Second, as shown in Tab. 4, comparing with previous methods employing the rectification modules [11, 36, 40, 54, 59, 61, 62] and the attention-based decoder [5, 25, 29, 31, 38, 47, 51, 52, 54, 56] to recognize irregular text, SVTRv2 also performs better than these methods on *Curve* and *MO*. In Fig. 4, the rectification module (*TPS*) and the attention-based decoder (*MAERec\**) do not recognize the extremely curved and rotated text correctly, in contrast, SMTR successes. Moreover, as demonstrated by the results on LTB in Tab. 4 and Fig. 5, *TPS* and *MAERec\** both do not effectively recognize long text, while SVTRv2 circumvents this limitation. These results indicate that our proposed modules successfully address the challenge of handling irregular text that existing CTC models encountered, while preserving CTC’s proficiency in recognizing long text.

SVTRv2 models also exhibit strong performance in Chinese text recognition (see Tab. 5), where SVTRv2-B achieve state of the art. The result underscores its great adaptability to different languages. To sum, we evaluate SVTRv2 across a wide range of scenarios. The results consistently confirm that this CTC model beats leading EDTRs.

## 5. Conclusion

In this paper, we have presented SVTRv2, an accurate and efficient CTC-based STR method. SVTRv2 is featured by

		R <sub>1</sub>	R <sub>2</sub>	R <sub>3</sub>	R <sub>4</sub>	Curve	MO	Com	U14M	LTB
	SVTRv2	<b>90.8</b>	<b>89.0</b>	<b>90.4</b>	<b>91.0</b>	<b>90.64</b>	<b>89.04</b>	<b>96.57</b>	<b>86.14</b>	<b>50.2</b>
TPS	SVTR [11]	86.8	82.3	77.3	75.7	82.19	86.12	94.62	78.44	0.0
	SVTRv2	89.5	85.1	78.4	83.8	84.71	88.97	94.62	79.94	0.5
MAERec*	SVTR [11]	81.3	87.6	87.6	88.3	87.88	78.74	96.32	83.23	0.0
	SVTRv2	88.0	88.9	89.4	88.3	89.96	87.56	96.42	85.67	0.2

Table 4. SVTRv2 and SVTR comparisons on irregular text and LTB, where the rectification module (*TPS*) and the attention-based decoder (*MAERec\**) are employed.

	CRNN	SVTR	LISTER	SVTRv2	w/ TPS	w/ MAERec*
	"SWEET LADY <b>IDOK</b> DOWN FROM THY <b>WOYDOW</b> ON <b>ME</b> "	"SWEET LADY LOOK DOWN FRO_ THY W_ NDOW OW ME,	"SWEET LADY LOOK _____ WINDOW ON ME?"	"SWEET LADY LOOK DOWN FROM THY WINDOW ON ME"	C	"mayLosMocanos.com
	EDITED WITH INTRODUCTION BY ROY TORGESON	EDITED W_ TH INTRODUCTION BY ROY TORGESON	EDITED WITH INTRODUCTION B_ O TORGESON	EDITED WITH INTRODUCTION BY ROY TORGESON	CIYYS	EDITED WITH IN _____ I_ N _____ G_ SON

Figure 5. Long text recognition results. *TPS* and *MAERec\** denote SVTRv2 integrated with *TPS* and the decoder of *MAERec*.

Method	Scene	Web	Doc	HW	Avg	Scene <sub>L&gt;25</sub>	Size
ASTER [40]	61.3	51.7	96.2	37.0	61.55	-	27.2
MORAN [32]	54.6	31.5	86.1	16.2	47.10	-	28.5
SAR [29]	59.7	58.0	95.7	36.5	62.48	-	27.8
SEED [36]	44.7	28.1	91.4	21.0	46.30	-	36.1
MASTER [31]	62.8	52.1	84.4	26.9	56.55	-	62.8
ABINet [15]	66.6	63.2	98.2	53.1	70.28	-	53.1
TransOCR [5]	71.3	64.8	97.1	53.0	71.55	-	83.9
CCR-CLIP [56]	71.3	69.2	98.3	60.3	74.78	-	62.0
DCTC [60]	73.9	68.5	99.4	51.0	73.20	-	40.8
CAM [54]	76.0	69.3	98.1	59.2	76.80	-	135
PARSeq* [4]	84.2	82.8	<b>99.5</b>	63.0	82.37	0.0	28.9
CPPD* [12]	82.7	82.4	99.4	62.3	81.72	0.0	32.1
MAERec* [25]	<b>84.4</b>	83.0	<b>99.5</b>	65.6	83.13	4.1	40.8
LISTER* [8]	79.4	79.5	99.2	58.0	79.02	13.9	55.0
CRNN* [39]	63.8	68.2	97.0	46.1	68.76	37.6	19.5
SVTR-B* [11]	77.9	78.7	99.2	62.1	79.49	22.9	19.8
SVTRv2-T	77.8	78.8	99.2	62.0	79.45	47.8	6.8
SVTRv2-S	81.1	81.2	99.3	65.0	81.64	50.0	14.0
SVTRv2-B	83.5	<b>83.3</b>	<b>99.5</b>	<b>67.0</b>	<b>83.31</b>	<b>52.8</b>	22.5

Table 5. Results on Chinese text dataset. \* denotes that the model is retrained using the same setting as SVTRv2 (Sec. 4.1).

developing the MSR and FRM modules to tackle the text irregular challenge, and devising the SGM module to endow linguistic context to the visual model. These upgrades maintain the simple architecture of CTC models, thus they remain quite efficient. More importantly, our thorough validation on multiple benchmarks demonstrates the effectiveness of SVTRv2. It achieves leading accuracy and inference



speed in various challenging scenarios covering regular, irregular, occluded, Chinese and long text, convincingly indicating that SVTRv2 has beat EDTRs in scene text recognition. In addition, we retrain 24 methods from scratch on *U14M-Filter* without data leakage, constituting a comprehensive and reliable benchmark. We hope that SVTRv2 and this benchmark will further advance the development of the OCR community.

## References

- [1] R. Anhar, S. Palaiahnakote, C. S. Chan, and C. L. Tan. A robust arbitrary text detection system for natural scene images. *Expert Syst. Appl.*, 41(18):8027–8048, 2014. [3](#), [5](#), [6](#)
- [2] J. Baek, G. Kim, J. Lee, S. Park, D. Han, S. Yun, S. J. Oh, and H. Lee. What is wrong with scene text recognition model comparisons? dataset and model analysis. In *ICCV*, pages 4714–4722, 2019. [2](#)
- [3] H. Bao, L. Dong, S. Piao, and F. Wei. BEiT: BERT pre-training of image transformers. In *ICLR*, 2022. [3](#)
- [4] D. Bautista and R.I. Atienza. Scene text recognition with permuted autoregressive sequence models. In *ECCV*, pages 178–196, 2022. [1](#), [2](#), [3](#), [5](#), [6](#), [7](#), [8](#)
- [5] J. Chen, B. Li, and X. Xue. Scene Text Telescope: Text-focused scene image super-resolution. In *CVPR*, pages 12021–12030, 2021. [7](#), [8](#)
- [6] J. Chen, H. Yu, J. Ma, M. Guan, X. Xu, X. Wang, S. Qu, B. Li, and X. Xue. Benchmarking chinese text recognition: Datasets, baselines, and an empirical study. *CoRR*, abs/2112.15093, 2021. [2](#), [5](#), [6](#)
- [7] X. Chen, L. Jin, Y. Zhu, C. Luo, and T. Wang. Text recognition in the wild: A survey. *ACM Comput. Surv.*, 54(2): 42:1–42:35, 2022. [1](#), [2](#)
- [8] C. Cheng, P. Wang, C. Da, Q. Zheng, and C. Yao. LISTER: Neighbor decoding for length-insensitive scene text recognition. In *ICCV*, pages 19484–19494, 2023. [1](#), [2](#), [7](#), [8](#), [3](#)
- [9] C. Da, P. Wang, and C. Yao. Levenshtein OCR. In *ECCV*, pages 322–338, 2022. [2](#), [3](#)
- [10] A. Dosovitskiy, L. Beyer, A. Kolesnikov, D. Weissenborn, X. Zhai, T. Unterthiner, M. Dehghani, M. Minderer, G. Heigold, S. Gelly, J. Uszkoreit, and N. Houlsby. An image is worth 16x16 words: Transformers for image recognition at scale. In *ICLR*, 2021. [7](#)
- [11] Y. Du, Z. Chen, C. Jia, X. Yin, T. Zheng, C. Li, Y. Du, and Y. Jiang. SVTR: Scene text recognition with a single visual model. In *IJCAI*, pages 884–890, 2022. [1](#), [2](#), [3](#), [4](#), [7](#), [8](#)
- [12] Y. Du, Z. Chen, C. Jia, X. Yin, C. Li, Y. Du, and Y. Jiang. Context perception parallel decoder for scene text recognition. *CoRR*, abs/2307.12270, 2023. [1](#), [2](#), [7](#), [8](#), [3](#)
- [13] Y. Du, Z. Chen, C. Jia, X. Gao, and Y. Jiang. Out of length text recognition with sub-string matching. *CoRR*, abs/2407.12317, 2024. [2](#), [5](#)
- [14] Y. Du, Z. Chen, Y. Su, C. Jia, and Y. Jiang. Instruction-guided scene text recognition. *CoRR*, abs/2401.17851, 2024. [3](#)
- [15] S. Fang, H. Xie, Y. Wang, Z. Mao, and Y. Zhang. Read Like Humans: Autonomous, bidirectional and iterative language modeling for scene text recognition. In *CVPR*, pages 7098–7107, 2021. [2](#), [3](#), [6](#), [7](#), [8](#)
- [16] A. Graves, S. Fernández, F. Gomez, and J. Schmidhuber. Connectionist temporal classification: Labelling unsegmented sequence data with recurrent neural networks. In *ICML*, page 369–376, 2006. [1](#)
- [17] T. Guan, C. Gu, J. Tu, X. Yang, Q. Feng, Y. Zhao, and W. Shen. Self-Supervised implicit glyph attention for text recognition. In *CVPR*, pages 15285–15294, 2023. [2](#), [3](#)
- [18] Tongkun Guan, Wei Shen, Xue Yang, Qi Feng, Zekun Jiang, and Xiaokang Yang. Self-Supervised Character-to-Character distillation for text recognition. In *ICCV*, pages 19473–19484, 2023. [2](#), [3](#)
- [19] A. Gupta, A. Vedaldi, and A. Zisserman. Synthetic data for text localisation in natural images. In *CVPR*, pages 2315–2324, 2016. [2](#), [7](#), [3](#)
- [20] K. He, X. Zhang, S. Ren, and J. Sun. Deep residual learning for image recognition. In *CVPR*, pages 770–778, 2016. [7](#), [1](#)
- [21] K. He, X. Chen, S. Xie, Y. Li, P. Dollár, and R. B. Girshick. Masked autoencoders are scalable vision learners. In *CVPR*, pages 15979–15988, 2022. [3](#)
- [22] A. G. Howard, M. Zhu, B. Chen, D. Kalenichenko, W. Wang, T. Weyand, M. Andreetto, and H. Adam. MobileNets: Efficient convolutional neural networks for mobile vision applications. *CoRR*, abs/1704.04861, 2017. [1](#)
- [23] W. Hu, X. Cai, J. Hou, S. Yi, and Z. Lin. GTC: Guided training of ctc towards efficient and accurate scene text recognition. In *AAAI*, pages 11005–11012, 2020. [1](#), [2](#), [3](#), [6](#)
- [24] M. Jaderberg, K. Simonyan, A. Vedaldi, and A. Zisserman. Synthetic data and artificial neural networks for natural scene text recognition. *CoRR*, abs/1406.2227, 2014. [2](#), [7](#), [3](#)
- [25] Q. Jiang, J. Wang, D. Peng, C. Liu, and L. Jin. Revisiting scene text recognition: A data perspective. In *ICCV*, pages 20486–20497, 2023. [1](#), [2](#), [3](#), [5](#), [6](#), [7](#), [8](#)
- [26] D. Karatzas, L. Gomez-Bigorda, A. Nicolaou, S. Ghosh, A. Bagdanov, M. Iwamura, J. Matas, L. Neumann, V. R. Chandrasekhar, S. Lu, F. Shafait, S. Uchida, and E. Valveny. ICDAR 2015 competition on robust reading. In *ICDAR*, pages 1156–1160, 2015. [5](#), [7](#)
- [27] D. KaratzasAU, F. ShafaitAU, S. UchidaAU, M. IwamuraAU, L. G. i. BigordaAU, S. R. MestreAU, J. MasAU, D. F. MotaAU, J. A. AlmazànAU, and L. P. de las Heras. ICDAR 2013 robust reading competition. In *ICDAR*, pages 1484–1493, 2013. [5](#), [6](#)
- [28] C. Li, W. Liu, R. Guo, X. Yin, K. Jiang, Y. Du, Y. Du, L. Zhu, B. Lai, X. Hu, D. Yu, and Y. Ma. PP-OCRv3: More attempts for the improvement of ultra lightweight ocr system. *CoRR*, abs/2206.03001, 2022. [1](#), [2](#), [3](#), [6](#)
- [29] H. Li, P. Wang, C. Shen, and G. Zhang. Show, attend and read: A simple and strong baseline for irregular text recognition. In *AAAI*, pages 8610–8617, 2019. [2](#), [3](#), [7](#), [8](#)
- [30] I. Loshchilov and F. Hutter. Decoupled weight decay regularization. In *ICLR*, 2019. [6](#)
- [31] N. Lu, W. Yu, X. Qi, Y. Chen, P. Gong, R. Xiao, and X. Bai. MASTER: Multi-aspect non-local network for scene text recognition. *Pattern Recognit.*, 117:107980, 2021. [7](#), [8](#)

- [32] C. Luo, L. Jin, and Z. Sun. MORAN: A multi-object rectified attention network for scene text recognition. *Pattern Recognit.*, 90:109–118, 2019. 2, 3, 4, 7, 8
- [33] A. Mishra, A. Karteek, and C. V. Jawahar. Scene text recognition using higher order language priors. In *BMVC*, pages 1–11, 2012. 5, 6
- [34] B. Na, Y. Kim, and S. Park. Multi-modal Text Recognition Networks: Interactive enhancements between visual and semantic features. In *ECCV*, pages 446–463, 2022. 2, 3, 7
- [35] T. Q. Phan, P. Shivakumara, S. Tian, and C. L. Tan. Recognizing text with perspective distortion in natural scenes. In *CVPR*, pages 569–576, 2013. 3, 5, 6
- [36] Z. Qiao, Y. Zhou, D. Yang, Y. Zhou, and W. Wang. SEED: Semantics enhanced encoder-decoder framework for scene text recognition. In *CVPR*, pages 13525–13534, 2020. 2, 3, 7, 8
- [37] M. Rang, Z. Bi, C. Liu, Y. Wang, and K. Han. An empirical study of scaling law for scene text recognition. In *CVPR*, pages 15619–15629, 2024. 2, 5
- [38] F. Sheng, Z. Chen, and B. Xu. NRTR: A no-recurrence sequence-to-sequence model for scene text recognition. In *ICDAR*, pages 781–786, 2019. 2, 3, 7, 8
- [39] B. Shi, X. Bai, and C. Yao. An end-to-end trainable neural network for image-based sequence recognition and its application to scene text recognition. *IEEE Trans. Pattern Anal. Mach. Intell.*, 39(11):2298–2304, 2017. 1, 3, 7, 8
- [40] B. Shi, M. Yang, X. Wang, P. Lyu, C. Yao, and X. Bai. ASTER: An attentional scene text recognizer with flexible rectification. *IEEE Trans. Pattern Anal. Mach. Intell.*, 41(9):2035–2048, 2019. 2, 3, 4, 7, 8
- [41] K. Simonyan and A. Zisserman. Very deep convolutional networks for large-scale image recognition. *CoRR*, abs/1409.1556, 2014. 1
- [42] A. Vaswani, N. Shazeer, N. Parmar, J. Uszkoreit, L. Jones, A. Gomez, Ł. Kaiser, and I. Polosukhin. Attention is all you need. In *NIPS*, pages 5998–6008, 2017. 4, 7
- [43] I. Loshchilov and F. Hutter. SGDR: stochastic gradient descent with warm restarts. In *ICLR*, 2017. 6
- [44] Z. Wan, F. Xie, Y. Liu, X. Bai, and C. Yao. 2d-ctc for scene text recognition. *CoRR*, abs/1907.09705, 2019. 2
- [45] K. Wang, B. Babenko, and S. Belongie. End-to-end scene text recognition. In *ICCV*, pages 1457–1464, 2011. 5, 6
- [46] P. Wang, C. Da, and C. Yao. Multi-Granularity Prediction for scene text recognition. In *ECCV*, pages 339–355, 2022. 2, 7, 3
- [47] T. Wang, Y. Zhu, L. Jin, C. Luo, X. Chen, Y. Wu, Q. Wang, and M. Cai. Decoupled attention network for text recognition. In *AAAI*, pages 12216–12224, 2020. 3, 7, 8
- [48] Y. Wang, H. Xie, S. Fang, J. Wang, S. Zhu, and Y. Zhang. From Two to One: A new scene text recognizer with visual language modeling network. In *ICCV*, pages 14194–14203, 2021. 2, 3, 5, 6, 7
- [49] J. Wei, H. Zhan, Y. Lu, X. Tu, B. Yin, C. Liu, and U. Pal. Image as a language: Revisiting scene text recognition via balanced, unified and synchronized vision-language reasoning network. In *AAAI*, pages 5885–5893, 2024. 2, 7, 3
- [50] S. Woo, S. Debnath, R. Hu, X. Chen, Z. Liu, I. S. Kweon, and S. Xie. Convnext V2: co-designing and scaling convnets with masked autoencoders. In *CVPR*, pages 16133–16142, 2023. 7
- [51] X. Xie, L. Fu, Z. Zhang, Z. Wang, and X. Bai. Toward Understanding WordArt: Corner-guided transformer for scene text recognition. In *ECCV*, pages 303–321, 2022. 2, 3, 7, 8
- [52] J. Xu, Y. Wang, H. Xie, and Y. Zhang. Ote: Exploring accurate scene text recognition using one token. In *CVPR*, pages 28327–28336, 2024. 2, 3, 7, 8
- [53] Jianwei Yang, Chunyuan Li, Xiyang Dai, and Jianfeng Gao. Focal modulation networks. In *NeurIPS*, 2022. 7
- [54] M. Yang, B. Yang, M. Liao, Y. Zhu, and X. Bai. Class-aware mask-guided feature refinement for scene text recognition. *Pattern Recognition*, 149:110244, 2024. 2, 3, 7, 8
- [55] D. Yu, X. Li, C. Zhang, T. Liu, J. Han, J. Liu, and E. Ding. Towards accurate scene text recognition with semantic reasoning networks. In *CVPR*, pages 12113–12122, 2020. 2, 3, 7
- [56] H. Yu, X. Wang, B. Li, and X. Xue. Chinese text recognition with a pre-trained CLIP-Like model through image-ids aligning. In *ICCV*, pages 11909–11918, 2023. 7, 8
- [57] X. Yue, Z. Kuang, C. Lin, H. Sun, and W. Zhang. RobustScanner: Dynamically enhancing positional clues for robust text recognition. In *ECCV*, pages 135–151, 2020. 2, 3, 7
- [58] B. Zhang, H. Xie, Y. Wang, J. Xu, and Y. Zhang. Linguistic More: Taking a further step toward efficient and accurate scene text recognition. In *IJCAI*, pages 1704–1712, 2023. 2, 3, 5, 7
- [59] H. Zhang, Q. Yao, M. Yang, Y. Xu, and X. Bai. AutoSTR: Efficient backbone search for scene text recognition. In *ECCV*, pages 751–767. Springer, 2020. 2, 3, 7, 8
- [60] Z. Zhang, N. Lu, M. Liao, Y. Huang, C. Li, M. Wang, and W. Peng. Self-distillation regularized connectionist temporal classification loss for text recognition: A simple yet effective approach. In *AAAI*, pages 7441–7449, 2024. 8, 3
- [61] Tianlun Zheng, Zheneng Chen, Jinfeng Bai, Hongtao Xie, and Yu-Gang Jiang. TPS++: Attention-enhanced thin-plate spline for scene text recognition. In *IJCAI*, pages 1777–1785, 2023. 2, 3, 8
- [62] T. Zheng, Z. Chen, S. Fang, H. Xie, and Y. Jiang. CDistNet: Perceiving multi-domain character distance for robust text recognition. *Int. J. Comput. Vis.*, 132(2):300–318, 2024. 2, 3, 7, 8
- [63] B. Zhou, Y. Qu, Z. Wang, Z. Li, B. Zhang, and H. Xie. Focus on the whole character: Discriminative character modeling for scene text recognition. *CoRR*, 2407.05562, 2024. 2, 3

# SVTRv2: CTC Beats Encoder-Decoder Models in Scene Text Recognition

## Supplementary Material

### 6. More detail of Ablation Study

SVTRv2 builds upon the foundation of SVTR by introducing several innovative strategies aimed at addressing challenges in recognizing irregular text and modeling linguistic context. The key advancements and their impact are systematically detailed below:

**Removal of the Rectification Module and Introduction of MSR and FRM.** In the original SVTR, a rectification module is employed to recognize irregular texts. However, this approach negatively impacts the recognition of long texts. To overcome this limitation, SVTRv2 removes the rectification module entirely. To effectively handle irregular text without compromising the CTC model’s ability to generalize to long text, MSR and FRM are introduced.

**Improvement in Feature Resolution.** SVTR extracts visual representations of size  $\frac{H}{16} \times \frac{W}{4} \times D_2$  from input images of size  $H \times W \times 3$ . While this approach is effective for regular text, it struggles with retaining the distinct characteristics of irregular text. SVTRv2 doubles the height resolution ( $\frac{H}{16} \rightarrow \frac{H}{8}$ ) of visual features, producing features of size  $\frac{H}{8} \times \frac{W}{4} \times D_2$ , thereby improving its capacity to recognize irregular text.

**Refinement of Local Mixing Mechanisms.** SVTR employs a hierarchical vision transformer structure, leveraging two mixing strategies: Local Mixing is implemented through a sliding window-based local attention mechanism, and Global Mixing employs the standard global multi-head self-attention mechanism. SVTRv2 retains the hierarchical vision transformer structure and the global multi-head self-attention mechanism for Global Mixing. For Local Mixing, SVTRv2 introduces a pivotal change. Specifically, the sliding window-based local attention is replaced with two consecutive group convolutions ( $\text{Conv}^2$ ). It is important to highlight that unlike previous CNNs [20, 22, 41], there is no normalization or activation layer between the two convolutions.

**Semantic Guidance Module (SGM).** The original SVTR model relies solely on CTC framework for both training and inference. However, CTC is inherently limited in its ability to model linguistic context. SVTRv2 addresses this by introducing a Semantic Guidance Module (SGM) during training. SGM facilitates the visual encoder in capturing linguistic information, enriching the feature representation. Importantly, SGM is discarded during inference, ensuring that the efficiency of CTC-based decoding remains unaffected while still benefiting from its contributions during the training phase.

### 6.1. Progressive Ablation Experiments

To comprehensively evaluate the contributions of the innovations in SVTRv2, a series of progressive ablation experiments are conducted. Tab 6 outlines the results, with the following observations:

1. Baseline (ID0): The original SVTR serves as the baseline for comparison.

2. Rectification Module Removal (ID1) reveals that while the rectification module (e.g., TPS) improves irregular text recognition accuracy, it hinders the model’s ability to recognize long texts. This confirms its limitations in balancing these tasks.

3. Improvement in Feature Resolution (ID2): Doubling the height resolution ( $\frac{H}{16} \rightarrow \frac{H}{8}$ ) significantly boosts performance across challenging datasets, particularly for irregular text.

4. Replacement of Local Attention with  $\text{Conv}^2$  (ID3): Replacing the sliding window-based local attention with two consecutive group convolutions ( $\text{Conv}^2$ ) yields improvements in artistic text, with a 3.0% increase in accuracy. This result highlights the efficacy of convolution-based approaches in capturing character-level nuances, such as strokes and textures, thereby improving its ability to recognize artistic and irregular text styles.

5. Incorporation of MSR and FRM (ID4 and ID5): These components collectively enhance accuracy on irregular text benchmarks (e.g., Curve), surpassing the rectification-based SVTR (ID0) by 6.0%, without compromising the CTC model’s ability to generalize to long text.

6. Integration of SGM (ID6): Adding SGM yields significant gains on multiple datasets, improving accuracy on OST by 5.11% and Union14M-Benchmark by 2.28%.

It can be summarized as that, by integrating  $\text{Conv}^2$ , MSR, FRM, and SGM, SVTRv2 significantly improves performance in recognizing irregular text and modeling linguistic context over SVTR, while maintaining robust long-text recognition capabilities and preserving the efficiency of CTC-based inference.

### 7. SVTRv2 Variants

There are several hyper-parameters in SVTRv2, including the depth of channel ( $D_i$ ) and the number of heads at each stage, the number of mixing blocks ( $N_i$ ) and their permutation. By varying them, SVTRv2 architectures with different capacities could be obtained and we construct three typical ones, i.e., SVTRv2-T (Tiny), SVTRv2-S (Small), SVTRv2-B (Base). Their detail configurations are shown in Tab. 7.

$[L]_m[G]_n$  denotes that the first  $m$  mixing blocks in

		IIIT5k	SVT	ICDAR2013	ICDAR2015	SVTP	CUTE80	Curve Multi-Oriented Artistic Contextless Salient Multi-Words General												
ID	Method	Common Benchmarks							Avg	Union14M Benchmarks						Avg	LTB	OST	Size	FPS
0	SVTR (w/ TPS)	98.1	96.1	96.4	89.2	92.1	95.8	94.62	82.2	86.1	69.7	75.1	81.6	73.8	80.7	78.44	0.0	71.2	19.95	141
1	0 + w/o TPS	98.0	97.1	97.3	88.6	90.7	95.8	94.58	76.2	44.5	67.8	78.7	75.2	77.9	77.8	71.17	45.1	67.8	18.10	161
2	$1 + \frac{H}{16} \rightarrow \frac{H}{8}$	98.9	97.4	97.9	89.7	91.8	96.9	95.41	82.2	64.3	70.2	80.0	80.9	80.6	80.5	76.95	44.8	69.5	18.10	145
3	2 + Conv <sup>2</sup> <sub>8</sub>	98.7	97.1	97.1	89.6	91.6	97.6	95.28	82.9	65.6	73.2	80.0	80.5	81.6	80.8	77.78	47.4	71.1	17.77	159
4	3 + MSR	98.7	98.0	97.4	89.4	91.6	97.6	95.44	87.4	83.7	75.4	80.9	81.9	83.5	82.8	82.22	50.9	72.5	17.77	159
5	4 + FRM	98.8	<b>98.1</b>	98.4	89.8	92.9	<b>99.0</b>	96.16	88.2	86.2	77.5	83.2	83.9	84.6	83.5	83.86	50.7	74.9	19.76	143
6	5 + SGM	<b>99.2</b>	98.0	<b>98.7</b>	<b>91.1</b>	<b>93.5</b>	<b>99.0</b>	<b>96.57</b>	<b>90.6</b>	<b>89.0</b>	<b>79.3</b>	<b>86.1</b>	<b>86.2</b>	<b>86.7</b>	<b>85.1</b>	<b>86.14</b>	<b>50.2</b>	<b>80.0</b>	19.76	143

Table 6. Ablation study of the proposed strategies on each benchmark subset, along with variations in the model parameters and speeds.

Models	$[D_0, D_1, D_2]$	$[N_1, N_2, N_3]$	Heads	Permutation
SVTRv2-T	[64,128,256]	[3,6,3]	[2,4,8]	$[L]_6[G]_6$
SVTRv2-S	[96,192,384]	[3,6,3]	[3,6,12]	$[L]_6[G]_6$
SVTRv2-B	[128,256,384]	[6,6,6]	[4,8,12]	$[L]_8[G]_{10}$

Table 7. Architecture specifications of SVTRv2 variants.

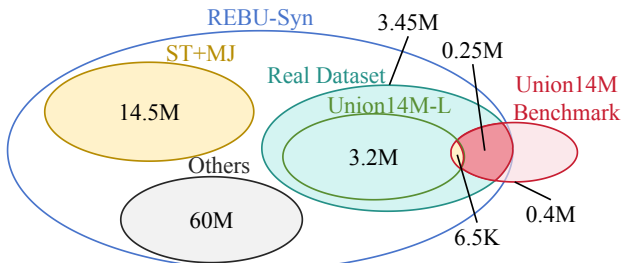


Figure 6. The relationship between the three real-world training sets.

	Curve	MO	Artistic	Cless	Salient	MW	General
	2,426	1,369	900	779	1,585	829	400,000
Real [4]	1,276	440	432	326	431	193	254,174
REBU-Syn [37]	1,285	443	462	363	442	289	260,575
U14M-Train [25]	9	3	30	37	11	96	6,401

Table 8. Overlapping analysis between the test set of Union14M-L (U14M) and three real-world training sets.

SVTRv2 utilize local mixing, while the last  $n$  mixing blocks employ global mixing. Specifically, in SVTRv2-T and SVTR-S, all blocks in the first stage and the first three blocks in the second stage use local mixing. The last three blocks in the second stage, as well as all blocks in the third stage, are global mixing. In the case of SVTRv2-B, all blocks in the first stage and the first two blocks in the second stage use local mixing, whereas the last four blocks in the second stage and all blocks in the third stage adopt global mixing.

### Algorithm 1: Inference Time

**Input** : A set of images  $\mathcal{I}$  with size  $|\mathcal{I}| = 3000$ , batch size  $B = 1$ ,  $N$  text lengths

**Output**: Overall inference time of the model

Initialize two lists: `total_time_list` and `count_list` of size  $N$ , initialized to 0;

**for** each image  $I_j$  in  $\mathcal{I}$  where  $j \in \{1, 2, \dots, 3000\}$  **do**

Determine the text length  $l_i$  for image  $I_j$ ;  
 Perform inference on  $I_j$  with text length  $l_i$ ;  
 Record inference time  $t_{ij}$ ;  
`total_time_list[li] += tij`;  
`count_list[li] += 1`;

Initialize `avg_time_list`;

**for** each text length  $l_i$  where  $i \in \{1, 2, \dots, N\}$  **do**

**if** `count_list[i] > 0` **then**  
`avg_time_list[i] =`  
`total_time_list[i] /`  
`count_list[i]`;

Compute the final average inference time:

$$\text{inference\_time} = \frac{1}{N} \sum_{i=1}^N \text{avg\_time\_list}[i]$$

**return** `inference_time`;

## 8. More detail of real-world datasets

For English recognition, we train models on real-world datasets, from which the models exhibit stronger recognition capability [4, 25, 37]. There are three large-scale real-world training sets, i.e., the *Real* dataset [4], *REBU-Syn* [37], and the training set of *Union14M-L* (*U14M-Train*) [25]. However, as shown in Fig. 6 and Tab. 8, the former two significantly overlap with Union14M-Benchmarks, thus not suitable for model training. Surprisingly, *U14M-Train* is also overlapped with Union14M-Benchmarks, in



IIIT5k SVT ICDAR2013 ICDAR2015 SVTP CUTE80    Curve Multi-Oriented Artistic Contextless Salient Multi-Words General																			
Method	Venue	Encoder	Common Benchmarks							Avg	Union14M Benchmarks							Avg	Size
ASTER [40]	TPAMI2019	ResNet+LSTM	93.3	90.0	90.8	74.7	80.2	80.9	84.98	34.0	10.2	27.7	33.0	48.2	27.6	39.8	31.50	27.2	
NRTR [38]	ICDAR2019	Stem+TF <sub>6</sub>	90.1	91.5	95.8	79.4	86.6	80.9	87.38	31.7	4.40	36.6	37.3	30.6	54.9	48.0	34.79	31.7	
MORAN [32]	PR2019	ResNet+LSTM	91.0	83.9	91.3	68.4	73.3	75.7	80.60	8.90	0.70	29.4	20.7	17.9	23.8	35.2	19.51	17.4	
SAR [29]	AAAI2019	ResNet+LSTM	91.5	84.5	91.0	69.2	76.4	83.5	82.68	44.3	7.70	42.6	44.2	44.0	51.2	50.5	40.64	57.7	
DAN [47]	AAAI2020	ResNet+FPN	93.4	87.5	92.1	71.6	78.0	81.3	83.98	26.7	1.50	35.0	40.3	36.5	42.2	42.1	32.04	27.7	
SRN [55]	CVPR2020	ResNet+FPN	94.8	91.5	95.5	82.7	85.1	87.8	89.57	63.4	25.3	34.1	28.7	56.5	26.7	46.3	40.14	54.7	
SEED* [36]	CVPR2020	ResNet+LSTM	93.8	89.6	92.8	80.0	81.4	83.6	86.87	40.4	15.5	32.1	32.5	54.8	35.6	39.0	35.70	24.0	
AutoSTR* [59]	ECCV2020	NAS+LSTM	94.7	90.9	94.2	81.8	81.7	-	-	47.7	17.9	30.8	36.2	64.2	38.7	41.3	39.54	6.00	
RoScanner [57]	ECCV2020	ResNet	95.3	88.1	94.8	77.1	79.5	90.3	87.52	43.6	7.90	41.2	42.6	44.9	46.9	39.5	38.09	48.0	
ABINet [15]	CVPR2021	ResNet+TF <sub>3</sub>	96.2	93.5	97.4	86.0	89.3	89.2	91.93	59.5	12.7	43.3	38.3	62.0	50.8	55.6	46.03	36.7	
VisionLAN [48]	ICCV2021	ResNet+TF <sub>3</sub>	95.8	91.7	95.7	83.7	86.0	88.5	90.23	57.7	14.2	47.8	48.0	64.0	47.9	52.1	47.39	32.8	
PARSeq* [4]	ECCV2022	ViT-S	97.0	93.6	97.0	86.5	88.9	92.2	92.53	63.9	16.7	52.5	54.3	68.2	55.9	56.9	52.62	23.8	
MATRAN [34]	ECCV2022	ResNet+TF <sub>3</sub>	96.6	95.0	97.9	86.6	90.6	93.5	93.37	63.1	13.4	43.8	41.9	66.4	53.2	57.0	48.40	44.2	
MGP-STR* [46]	ECCV2022	ViT-B	96.4	94.7	97.3	87.2	91.0	90.3	92.82	55.2	14.0	52.8	48.5	65.2	48.8	59.1	49.09	148	
LevOCR* [9]	ECCV2022	ResNet+TF <sub>3</sub>	96.6	94.4	96.7	86.5	88.8	90.6	92.27	52.8	10.7	44.8	51.9	61.3	54.0	58.1	47.66	109	
CornerTF* [51]	ECCV2022	CornerEncoder	95.9	94.6	97.8	86.5	91.5	92.0	93.05	62.9	18.6	56.1	58.5	68.6	59.7	61.0	55.07	86.0	
CPPD [12]	Preprint	SVTR-B	97.6	95.5	98.2	87.9	90.9	92.7	93.80	65.5	18.6	56.0	61.9	71.0	57.5	65.8	56.63	26.8	
SIGA* [17]	CVPR2023	ViT-B	96.6	95.1	97.8	86.6	90.5	93.1	93.28	59.9	22.3	49.0	50.8	66.4	58.4	56.2	51.85	113	
CCD* [18]	ICCV2023	ViT-B	97.2	94.4	97.0	87.6	<b>91.8</b>	93.3	93.55	66.6	24.2	<b>63.9</b>	64.8	74.8	62.4	64.0	60.10	52.0	
LISTER* [8]	ICCV2023	FocalNet-B	96.9	93.8	97.9	87.5	89.6	90.6	92.72	56.5	17.2	52.8	63.5	63.2	59.6	65.4	54.05	49.9	
LPV-B* [58]	IJCAI2023	SVTR-B	97.3	94.6	97.6	87.5	90.9	94.8	93.78	68.3	21.0	59.6	65.1	76.2	63.6	62.0	59.40	35.1	
CDistNet* [62]	IJCV2024	ResNet+TF <sub>3</sub>	96.4	93.5	97.4	86.0	88.7	93.4	92.57	69.3	24.4	49.8	55.6	72.8	64.3	58.5	56.38	65.5	
CAM* [54]	PR2024	ConvNeXtV2-B	97.4	<b>96.1</b>	97.2	87.8	90.6	92.4	93.58	63.1	19.4	55.4	58.5	72.7	51.4	57.4	53.99	135	
BUSNet [49]	AAAI2024	ViT-S	96.2	95.5	<b>98.3</b>	87.2	<b>91.8</b>	91.3	93.38	-	-	-	-	-	-	-	56.8		
DCTC [60]	AAAI2024	SVTR-L	96.9	93.7	97.4	87.3	88.5	92.3	92.68	-	-	-	-	-	-	-	40.8		
OTE [52]	CVPR2024	SVTR-B	96.4	95.5	97.4	87.2	89.6	92.4	93.08	-	-	-	-	-	-	-	25.2		
CRNN [39]	TPAMI2016	ResNet+LSTM	82.9	81.6	91.1	69.4	70.0	65.5	76.75	7.50	0.90	20.7	25.6	13.9	25.6	32.0	18.03	8.30	
SVTR* [11]	IJCAI2022	SVTR-B	96.0	91.5	97.1	85.2	89.9	91.7	91.90	69.8	<b>37.7</b>	47.9	61.4	66.8	44.8	61.0	55.63	24.6	
SVTRv2	-	SVTRv2-B	<b>97.7</b>	94.0	97.3	<b>88.1</b>	91.2	<b>95.8</b>	<b>94.02</b>	<b>74.6</b>	25.2	57.6	<b>69.7</b>	<b>77.9</b>	<b>68.0</b>	<b>66.9</b>	<b>62.83</b>	19.8	

Table 9. Results of SVTRv2 and existing models when trained on synthetic datasets ( $ST + MJ$ ) [19, 24]. \* represents that the results on Union14M-Benchmarks are evaluated using the model they released.

nearly 6.5k text instances across the seven subsets. It means the models trained based on  $U14M-Train$  suffer from data leakage when tested on Union14M-Benchmarks, thus the results reported by [25] should be updated. To this end, we create a filtered version of Union14M-L training set, termed as  $U14M-Filter$ , by filtering these overlapping instances. This new dataset is used to train SVTRv2 and other 24 methods we reproduced.

## 9. More detail of Inference Time

In term of the inference time, we do not utilize any acceleration framework and instead employ PyTorch’s dynamic graph mode on one NVIDIA 1080Ti GPU. We first measure the inference time for 3,000 images with a batch size of 1, calculating the average inference time for each text length. We then computed the arithmetic mean of the average time across all text lengths to determine the overall inference time of the model. Algorithm 1 details the process of measuring inference time.

## 10. Results when trained on synthetic datasets

Previous research typically follows a typical evaluation protocol, where models are trained on synthetic datasets and validated using six widely recognized real-world benchmarks. Building on this protocol, we trained the SVTRv2 model on synthetic datasets. In addition to evaluating SVTRv2 on the six common benchmarks, we also assess its performance on challenging benchmarks, i.e. Union14M-Benchmark, offering a comprehensive understanding of the model’s generalization capabilities. For methods that have not reported performance on challenging benchmarks, we conducted additional evaluations using their publicly available models and present these results for comparative analysis. As illustrated in Tab. 9, models trained on synthetic datasets exhibit notably reduced performance compared to those trained on large-scale real-world datasets (see Tab. 3). This performance drop is particularly pronounced on challenging benchmarks. These findings emphasize the critical importance of real datasets in improving recognition accuracy for challenging text scenarios.

Despite the challenges associated with synthetic datasets, SVTRv2 exhibits superior performance across

	Blurred	Artistic	Incomplete	Other	Total	Label <sub>err</sub>
IIIT5k	0	16	1	4	21	4
SVT	4	4	4	0	12	0
ICDAR 2013	2	2	4	2	10	2
ICDAR 2015	48	19	42	13	122	35
SVTP	7	6	12	7	32	4
CUTE80	0	1	0	0	1	1
Total	61	48	63	26	198	46
	30.81%	24.24%	31.82%	13.13%	100%	

Table 10. Distribution of bad cases for SVTRv2 on *Common* benchmarks.

both average accuracy metrics, surpassing the previously best-performing method by 0.22% and 2.73%, respectively. On irregular text benchmarks, such as *Curve* and *Multi-Oriented*, SVTR achieves strong results, largely due to its integrated correction module, which is particularly adept at handling irregular text patterns, even when trained on synthetic datasets. Notably, SVTRv2 achieves a substantial 4.8% improvement over SVTR on the *Curve* benchmark, further demonstrating its enhanced capacity to address irregular text. Overall, these results demonstrate that, even when trained solely on synthetic datasets, SVTRv2 exhibits strong generalization capabilities, effectively handling complex and challenging text recognition scenarios.

## 11. Qualitative Analysis of Recognition Results

The SVTRv2 model achieved an average accuracy of 96% on a standard dataset. To investigate the underlying causes of the remaining 4% of recognition errors, we conducted a detailed analysis of misclassified samples across six standard datasets, as illustrated in Fig. 7 and Fig. 8. While previous research has typically categorized common benchmarks into *regular* and *irregular* text. However, these error samples indicates that the majority of incorrectly recognized text is not irregular. This suggests that, under the current training paradigm using large-scale real-world datasets, a more rigorous manual screening process for common benchmarks is warranted.

Consequently, we identified five primary causes of recognition errors in these samples: (1) blurred, (2) artistic, (3) incomplete text, (4) image text labeling inconsistency, and (5) others. Specifically, the blurring text category encompasses issues such as low resolution, motion blur, or extreme lighting conditions. The artistic text category includes unconventional print fonts, predominantly found in business signage, as well as a proportion of handwritten text. Incomplete text refers to characters obscured by other objects or missing due to improper cropping, where missing information must be inferred from context. Image text labeling inconsistency means that there is an error in the given text label or there are some characters with phonetic sym-

bols. As shown in Tab. 10, after excluding samples where the errors were due to labeling inconsistency, the remaining errors could be attributed to blurred (30.81%), artistic (24.24%), and incomplete text (31.82%), respectively. This classification allows us to conclude that SVTRv2’s recognition performance, particularly in complex scenarios involving blurred, artistic, or incomplete text, requires further enhancement.

## 12. Standardized Model Training Settings

The optimal hyperparameters for training different models often vary and are not universally fixed. However, critical factors such as training epochs, data augmentation techniques, input size, data type, and evaluation protocols have a substantial influence on model accuracy. To ensure fair and unbiased performance comparisons across models, these factors must be strictly standardized. Accordingly, we adopt a uniform training and evaluation setting, as shown in Table 11, to maintain consistency across all settings while simultaneously enabling each model to achieve its best possible accuracy.

<b>Setting</b>	<b>Detail</b>
<b>Training Set</b>	For training, when the text length of a text image exceeds 25, samples with text length $\leq 25$ are randomly selected from the training set to ensure models are only exposed to short texts (length $\leq 25$ ).
<b>Test Sets</b>	For all test sets except the long-text test set (LTB), text images with text length $> 25$ are filtered. Text length is calculated by removing spaces and non-94-character-set special characters.
<b>Input Size</b>	Unless a method explicitly requires a dynamic size, models use a fixed input size of $32 \times 128$ . If a model performs incorrectly with $32 \times 128$ during training, the original size is used. The test input size matches the training size.
<b>Data Augmentation</b>	All models use the data augmentation strategy employed by PARSeq.
<b>Training Epochs</b>	Unless pre-training is required, all models are trained for 20 epochs.
<b>Optimizer</b>	AdamW is the default optimizer. If training fails to converge with AdamW, Adam or other optimizers are used.
<b>Batch Size</b>	Maximum batch size for all models is 1024. If single-GPU training is not feasible, 2 GPUs (512 per GPU) or 4 GPUs (256 per GPU) are used. If 4-GPU training runs out of memory, the batch size is halved, and the learning rate is adjusted accordingly.
<b>Learning Rate</b>	Default learning rate for batch size 1024 is 0.00065. The learning rate is adjusted multiple times to achieve the best results.
<b>Learning Rate Scheduler</b>	A linear warm-up for 1.5 epochs is followed by a OneCycle scheduler.
<b>Weight Decay</b>	Default weight decay is 0.05. NormLayer and Bias parameters have a weight decay of 0.
<b>Data Type</b>	All models are trained with mixed precision.
<b>EMA or Similar Tricks</b>	No EMA or similar tricks are used for any model.
<b>Evaluation Protocols</b>	Word accuracy is evaluated after filtering special characters and converting all text to lowercase.

Table 11. A uniform training and evaluation setting to maintain consistency across all settings while simultaneously enabling each model to achieve its best possible accuracy.



Figure 7. The bad cases of SVTrv2 in IIIT5k [33], SVT [45], ICDAR 2013 [27], SVTP [35] and CUTE80 [1]. labels and predicted results, and predicted scores are denoted as  $Text_{label} | Text_{pred} | Score_{pred}$ . Yellow, red, blue, and green boxes indicate blurred, artistic fonts, incomplete text, and label-inconsistent samples, respectively. Other samples have no boxes.





Figure 8. The bad cases of SVTRv2 in ICDAR 2015 [26]. labels and predicted results, and predicted scores are denoted as  $\text{Text}_{\text{label}} | \text{Text}_{\text{pred}} | \text{Score}_{\text{pred}}$ . Yellow, red, blue, and green boxes indicate blurred, artistic fonts, incomplete text, and label-inconsistent samples, respectively. Other samples have no boxes.